Mechanics of Advanced Composite Structures 9 (2022) 287 – 296

Semnan University

Mechanics of Advanced Composite Structures

journal homepage: http://MACS.journals.semnan.ac.ir

Deposition of an Al/SiC Composite Coating on Steel by Friction Surfacing: Corrosion and Wear Properties

A. Tabaghi [a], H. Tavakoli [b*], A. Kami [a]

[a] *Faculty of Mechanical Engineering, Semnan University, Semnan, Iran*
[b] *Faculty of Materials and Metallurgical Engineering, Semnan University, Semnan, Iran*

KEYWORDS

Friction surfacing;
Wear resistance;
Corrosion properties;
Al/Sic composite coating;
EIS.

ABSTRACT

Friction Surfacing (FS) is a method to create coatings on surfaces, a commonly used approach for improving the surface properties of materials. This study investigated the deposition of an Al/SiC composite coating of AA2030 aluminum alloy and 250 µm SiC particles on a plain carbon steel substrate by FS. Holes of a 3.5 mm diameter were made in the AA2030 rod and filled with SiC powder. This consumable rod was then pressed on the surface of an St37 plate with an axial force of 450 N. The rod was rotated and moved around to coat the surface of the St37 substrate with a layer of Al/SiC composite. The results showed that SiC particles break down and get evenly dispersed over the surface. The deposited composite coating offered 41.6% better wear resistance and up to 70% better corrosion resistance than the non-composite coating. The electrochemical impedance analysis showed two time constants in the Nyquist plots.

1. Introduction

Surface coating processes are widely used in numerous industries, including aerospace, automotive, oil and gas extraction, and processing. These processes aim to improve the surface's mechanical properties (e.g., wear resistance), metallurgical properties, or electrochemical properties. Over the years, various coating methods, including powder metallurgy, laser cladding, chemical vapor deposition (CVD), nitriding, and physical vapor deposition (PVD), have been developed for this purpose [1, 2]. The FS process was introduced more than fifty years ago but has remained largely dormant. Although the process received some attention in the United Kingdom in the 1980s, it was never seriously used. However, in recent years, the success of friction stir welding (FSW) and the need for alternative coating processes have led to renewed interest in the FS process [3]. The coating created by the FS process improves the substrate's mechanical and metallurgical properties (e.g., corrosion resistance and wear resistance) [4]. Since one way to improve the strength of light alloys relative to their density is to add reinforcements such as fiber or particles to their composition [5], there have been many efforts to find cost-effective methods of creating high-quality composite coatings on alloys. One of these methods is friction stir processing (FSP). A non-consumable stirring tool is forcibly applied to a surface, causing friction-induced deformations at high temperatures and microstructural changes in the deformed area [6]. According to studies on the deposition of aluminum coatings on steel surfaces by FSP, this process improves the corrosion resistance of these surfaces [7].

Typically, the cross-section of the coating created by FS is free of surface defects such as holes, pores, and porosity [8]. In FS, the substance deposited on the substrate is in the form of a rod consumed during the process. With the metal substrate well clamped, the consumable rod is rotated on the substrate surface under a constant axial force, creating intense friction at the rod-substrate interface. This friction generates intense local heat, which, along with the axial force, causes plastic deformation in the rod. After a short time, the substrate moves forward, causing part of the plastically deformed consumable rod to remain welded on the surface. As the substrate moves, a coating layer is deposited directly on the surface of the base metal [9]. All the heat required for this process is

*Corresponding Author. Tel.: +98-23-31532380 ; Fax: +98-23-31532335
E-mail address: h.tavakoli@semnan.ac.ir

DOI: 10.22075/macs.2022.26221.1383
Received 2022-02-07; Received in revised form 2022-06-14; Accepted 2022-08-26

generated by the friction between the consumable rod and the substrate, which means there is no need for a separate heat generator. Thus, FS can be described as a coating process with a degree of energy consumption control [9]. The coating's interfacial properties revealed that it is metallurgically attached to the substrate without dilution. This is the advantage of the FS method over other coating methods. Metallurgical bonding was obtained by combining the two nascent surfaces generated by eliminating oxide layers due to intense rubbing under compressive strain [10].

The past studies on the deposition of aluminum coatings on steel surfaces by FSP have shown that it leads to enhanced corrosion resistance [11]. Also, aluminum alloys reinforced with ceramic particles have been shown to have remarkable strength, hardness, and low density [11, 12]. These properties make ceramic particle-reinforced composites suitable for parts requiring high strength, hardness, and low density [13]. Since one of the primary purposes of coatings is to prevent corrosion, when assessing the applicability of a coating, it is essential to examine its behavior in corrosive environments. The FS process can also create a corrosion-resistant coating on a substrate. However, reinforcing particles can significantly impact the resulting coating's physical, chemical, and electrochemical properties [14]. It has been reported that corrosion-induced cavities start from the pores in the coating matrix. In general, composites have more pores and cavities than non-composite matrices. Thus, corrosion resistance decreases with the increasing volume of ceramic particles in the coating [15].

Ranjan and Das [16] discuss several substrates' mechanical and corrosion protection characteristics following the FS process; examples are as follows: Bararpour et al. [17] investigated the effects of non-isothermal aging on the microstructure and mechanical properties of the composite AA5083-15 wt% Zn coating applied to AA5052. The precipitation hardening mechanism was revealed to be the primary mechanism responsible for enhancing the hardness and strength of the zinc-rich coating during the non-isothermal aging phase. Sahoo et al. [18, 19] deposited AA6063 on the surface of EN8 [18] and AISI304 [19] steels using the FS technique. They studied the effects of the tool's rotational speed, feed rate, axial force, and substrate preheating on coating dimensions and bonding strength. They achieved optimal process parameters, which resulted in the most robust bonding strength. A comparable study was conducted on FS of IS2062 mild steel coated with AA6351 [20]. Yu et al. [21] FSed AA6061 on the surface of Q235 carbon steel. They discovered that intermetallic particles dispersed randomly; they obtained a highly refined coating, and the coating's corrosion resistance was increased.

The literature analysis suggests that the coating of steel with various aluminum alloys has received little attention. Additionally, aluminum composites have unique properties [22], making them attractive for supporting coating applications. Thus, this work aims to use the FS method to create an Al/SiC composite coating on a steel substrate and investigate the coating's wear, microscopic, and electrochemical properties.

2. Materials and Method

2.1. Materials

In this study, plain carbon steel plates (St37) of size 100 × 50 × 5 mm^3 were used as the substrate, aluminum 2030 (AA2030) was used as the consumable rod, and 250-micron silicon carbide powder with 99% purity was used as the reinforcing particle.

2.2. The Composite Coating Deposition Method

The coating was deposited using a vertical milling machine. Figure 1 illustrates how the consumable rod was mounted on the machine and the substrate clamped on the machine's table.

Figure 2a shows that the consumable rod was fitted inside a holder and under an axial force of 450 N. This holder was clamped inside the milling machine's spindle (see Fig. 3).

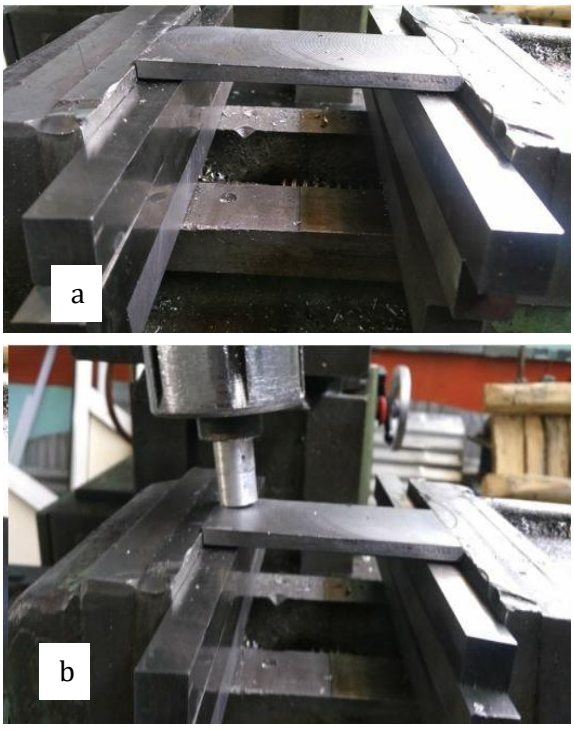

Fig. 1. a) Clamping of the substrate on the table of the milling machine b) Mounting of the consumable rod on the milling machine

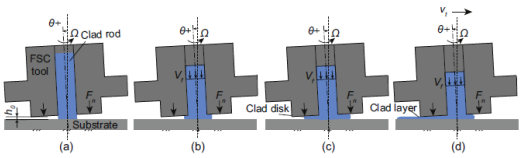

Fig. 2. Schematic of coating deposition with the FS method [4]

Fig. 3. The rod holder's bottom (left) and side (right) views

The spindle angle, rotation speed, and feed rate were set to 6°, 800 rpm, and 60 mm/min, respectively. After checking to ensure all parameters were correctly set and all parts were appropriately clamped, the machine was adjusted to have a minimum distance of 1 mm between the edge of the rod holder and the surface of the substrate.

After turning on the machine, a 450 N axial force was applied to the rotating rod until it showed plastic deformation (Fig. 2b). At that point, the forward motion of the machine's table was triggered to start (Fig. 2c). The rod moved over the substrate, leaving a coating layer on the surface. In this process, the tool shoulder determines the thickness of the created coating and the smoothness of the surface (Fig. 2d).

The silicon carbide particles had to be mixed with the alloy to create a composite coating. For this purpose, as shown in Fig. 4, one or two holes with a 3.5 mm diameter were created in the rod and filled with silicon carbide powder. The created specimens were named as shown in Table 1. The first case is considered with one hole (sample S3 in Table 1) and the second case with two holes (sample S4 in Table 1). The volume percentage of SiC particles equals the ratio of the hole area to the drilled aluminum rod area. Accordingly, the volume percentages of SiC particles in samples S3 and S4 equal 6.19% and 13.19%, respectively.

2.3. Coating Examination Methods

To eliminate the effects of initial irregularities in the coating process on the results, the first 30 mm of all specimens were cut out. After that, the specimens were cut into 10 mm long pieces. The coated surfaces were examined with an FEI Quanta450 electron microscope equipped with an EDS detector model Oxford Ultim Max Large Area SDD.

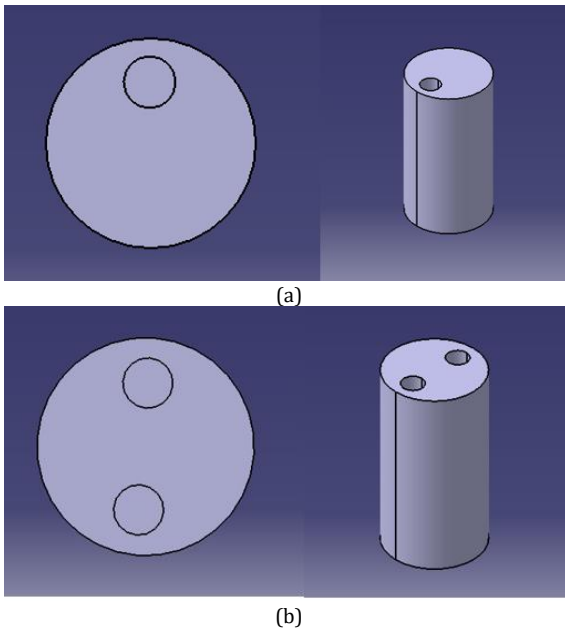

(a)

(b)

Fig. 4. The consumable road with (a) one hole and (b) two holes

Table 1. The manufactured specimens and their characteristics

Specimen Name	Substrate/Coating	Volume percentage of SiC	Coating's density (g/cm^3)
S1	Steel (uncoated)	-	-
S2	Steel/Aluminum	0	2.70
S3	Steel/Composite coating made with one hole in the rod	6.19	2.73
S4	Steel/Composite coating made with two holes in the rod	13.19	2.77

Wear testing was performed using the pin-on-disk method with a 3 mm pin made of AISI 52100 Chrome Steel with a hardness of 65 HRC. In this test, the axial force was 20 N, the pin sliding speed was 0.05 m/s, and the sliding distance was 300 m. The weight of the specimens before and after the wear test was measured with an A&D Weighing GR-120 laboratory scale. The disc specimens needed for this wear test were prepared in the dimensions 10 × 2 × 15 mm^3 with a 5mm thick coating.

Electrochemical tests were performed in a flat cell manufactured by EG&G, where 1 cm^2 of the specimen gets exposed to the electrolyte. The temperature for all electrochemical tests was 25°C. The Tafel and open-circuit potential tests (Eocp) were conducted in an Origa Flex OGF500 potentiostat. The reference electrode was SCE (Saturated Calomel Electrode), and the auxiliary electrode was platinum with a surface area of 5

cm^2. In the Tafel polarization test, the applied potential was changed from -550 to -900 mV, and the scanning rate was one mV/s. The extrapolation of Tafel lines determined the corrosion current density. The Electrochemical Impedance Spectroscopy (EIS) tests were also performed in an Origa Flex OGF500 potentiostat with frequencies ranging from 10 kHz to 10 MHz and sine wave voltages in the range of ±10 mV relative to Eocp.

3. Results and Discussions

3.1. Microscopic Examination

The EDS images of the specimens S2, S3, and S4 are depicted in Fig. 5. As shown in Fig. 5a, the surface coated with pure aluminum did not have any sign of silicon element.

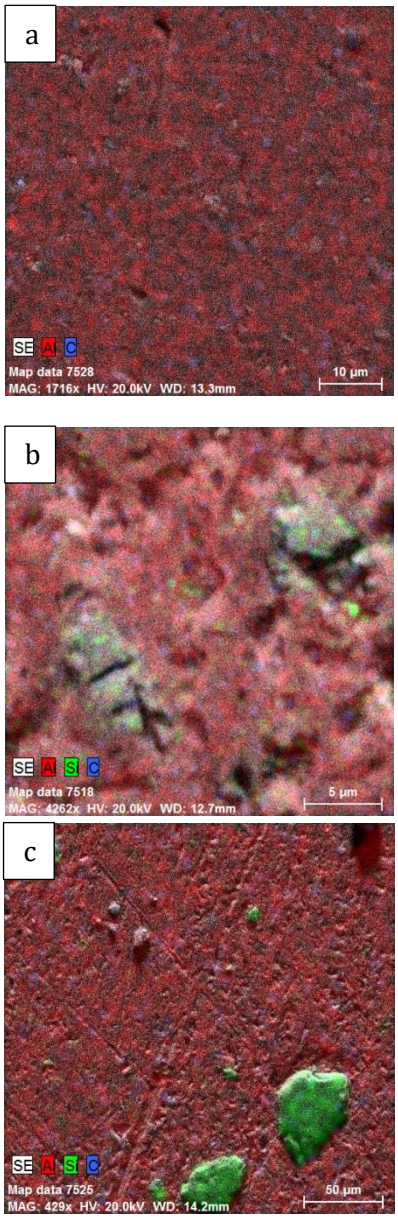

Fig. 5. MAP images taken from the specimens (a) S2, (b) S3, and (c) S4

Figure 5b shows the coating created when one hole in the rod was filled with SiC micro-powder (specimen S3). As can be seen, SiC particles are well dispersed on the surface of this specimen. In Fig. 5c, which shows the coating created while having two SiC-filled holes in the rod, there are clear signs of large amounts of silicon on the surface. As the amount of reinforcing particles in the coating increases, so does the hardness of the formed layer [23]. Thus, having two SiC-filled holes in the consumable rod increases the product's hardness by ensuring that higher amounts of reinforcing particles are present on the composite surface.

Figure 6 illustrates the SEM images taken from the surface of the coated specimens S2, S3, and S4. Given the size of the reinforcing particles, it is clear that they were very equally broken down during the process. As can be seen, the particle size has decreased from 250 microns to approximately 5 microns, and the particles have become well dispersed over the surface. Figure 6c shows the SEM image of the coating surface produced by the rod with two SiC-filled holes. SiC particles are more refined in this specimen than in the first specimen. The particle diameter has decreased from 250 to about 50 microns, and particles are almost evenly distributed over the surface. By comparing Fig. 5b and Fig. 6c, one can see that the reinforcing particles in Fig. 6b are much smaller and are more uniformly dispersed on the coating surface. Therefore, it is clear that the stresses applied to the reinforcing particles at the surface-rod interface have caused these particles to break down. According to these results, a smaller amount of powder results in a more extensive crushing of SiC particles and, therefore, smaller particles in the product.

The dispersion of silicon and carbon on specimens S2 and S3's surface suggests the dispersion of SiC particles on these coatings (Fig. 7). As shown in Fig. 7, SiC particles have been crushed during the coating operation. A comparison of Figs. 7a and 7b show that in specimen S3, where lower amounts of SiC powder have been introduced, particles are more crushed, and fewer coarse particles are on the surface. More uniform dispersion of the reinforcing particles on the surface will have more uniform properties over the produced composite. Figure 6 also shows that specimen S3, which has a lower SiC content than S4, has a more uniform particle distribution on the surface, with far fewer large SiC particles. Therefore, it can be concluded that specimen S3, created with one SiC-filled hole in the consumable rod, has smaller reinforcing particles with better dispersion and more uniform distribution over the surface.

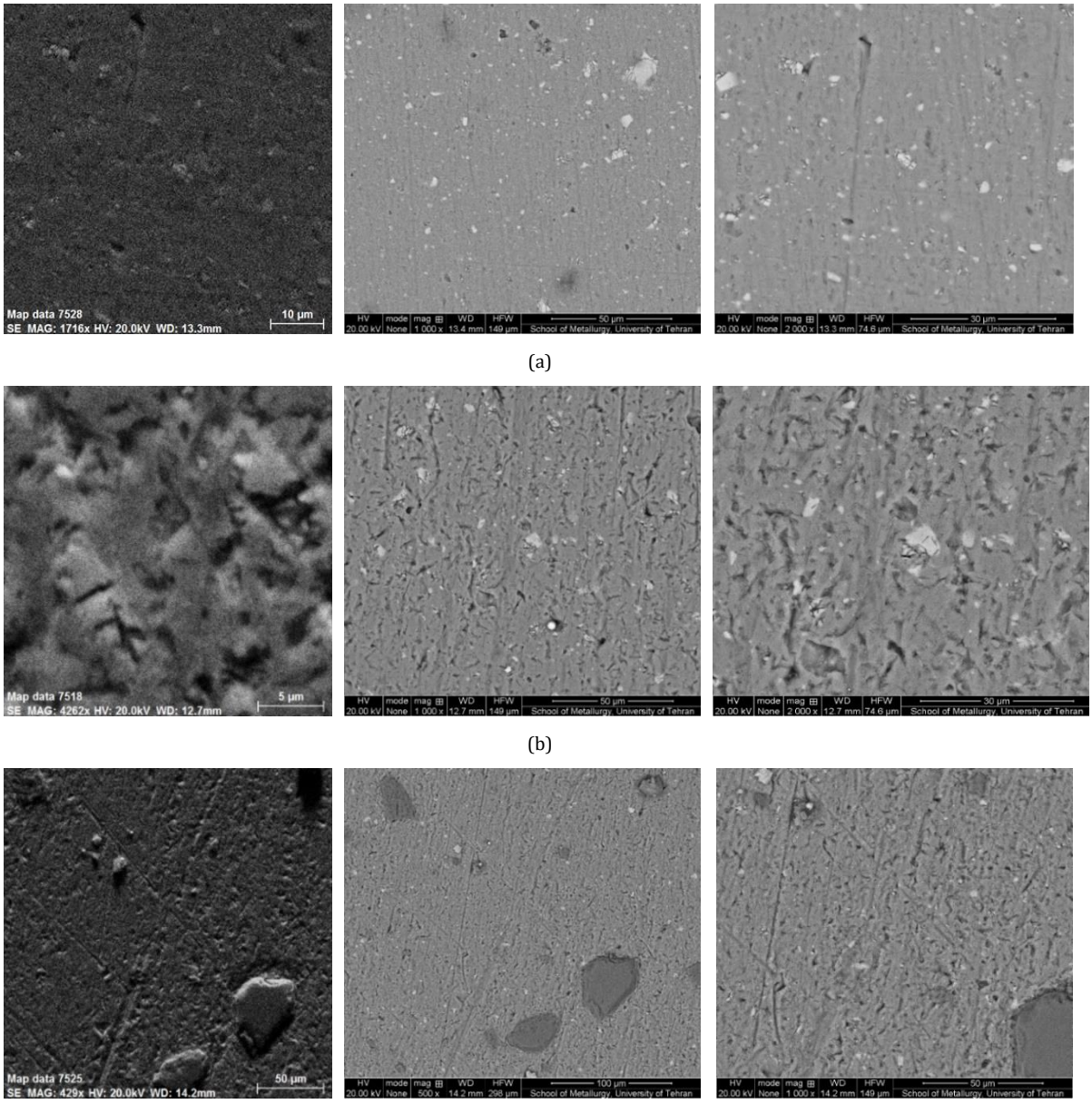

(a)

(b)

(c)

Fig. 6. SEM images taken from the surface of the specimens (a) S2, (b) S3, and (c) S4 at different magnification levels

3.2. Examination of Wear Resistance Properties

The pin-on-disk test was performed to examine the wear properties of the specimens. With an axial force of 20 N, a sliding speed of 0.05 m/s, and a sliding distance of 300 m, a pin diameter of 3 mm was driven onto the surface. The changes in the mass of the specimens and pins are given in Table 2. As can be seen, there was almost no change in the mass of the pins during the tests. But there were measurable changes in the mass of all specimens before and after this test. These results showed more significant mass changes in specimen S2 (which had no reinforcing powder) than S3 (which had a small amount of this powder). They also showed that specimen S3 experienced more significant mass changes than S4 (with a higher reinforcing powder). These results suggest that higher amounts of reinforcing powder on the coating surface lead to improved wear resistance, as indicated by more minor mass changes in the pin-on-disk test.

The diagrams in Fig. 8 show the coefficient of friction in terms of the sliding distance. In all of these diagrams, the curves can be divided into three parts: they ascend in the first 10 meters until reaching a peak and then remain almost constant until the end. There are minor disruptions in this trend, which could be due to the wear adhesion, i.e., the pin continuously sticking to and getting detached from the surface, or the presence of SiC particles that are not evenly distributed over the surface.

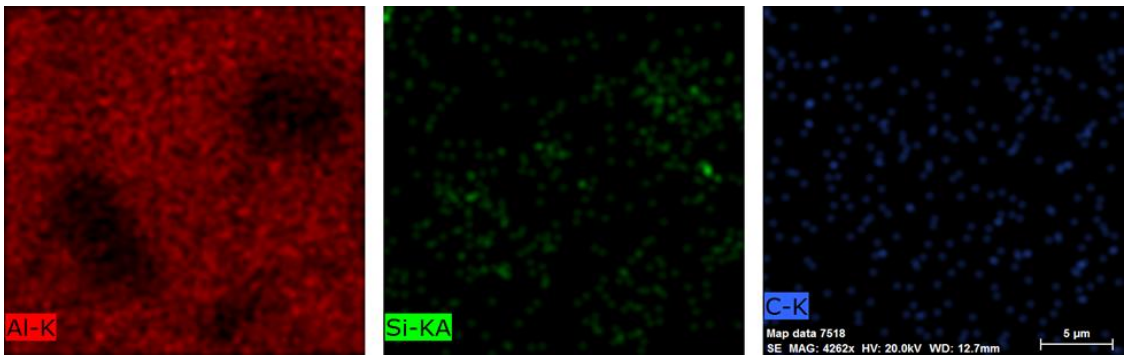

(a)

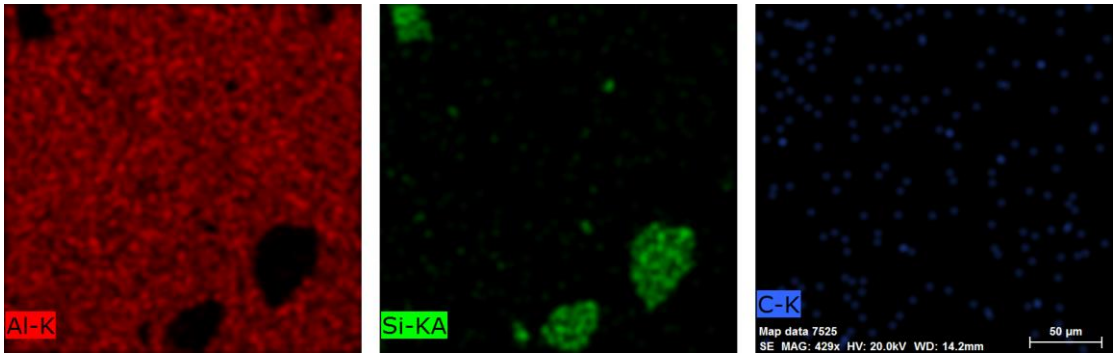

(b)

Fig. 7. Dispersion of the constituting particles of the coating in the specimens (a) S3 and (b) S4

Table 2. Change in the mass of pins and specimens in the pin-on-disk test

Specimen	Number of holes in the consumable rod	The initial mass of the specimen (g)	The final mass of the specimen (g)	Change in the mass of the specimen (g)	Change in the mass of the pin (g)
S2	0	27.5575	27.5470	0.0105	0.0000
S3	1	19.8904	19.8860	0.0086	0.0000
S4	2	11.0462	11.0388	0.0074	0.0001

By comparing the diagrams in Fig. 8, one can see that as the amount of reinforcing powder increases, the coefficient of friction decreases. The average value of the coefficient of friction in the steady part of the curve are 0.62, 0.58, and 0.55 for samples S2, S3, and S4, respectively. In other words, increasing the SiC content increases the resistance of the produced coating to surface wear.

The wear properties of the coatings were studied by performing the pin-on-disk test. The changes in the mass of coated specimens and the pins are given in Table 2. From the results presented in Table 2, it can be concluded that the higher the amount of reinforcing particles in the coating, the smaller the change in the mass of the specimen will be. The plots of friction coefficient versus sliding distance for the specimens S2, S3, and S4 are drawn in Fig. 8. This figure shows that the higher the amount of reinforcing particles in the coating, the lower the coefficient of friction. From Table 2 and Fig. 8, it can be concluded that as the SiC content of the coating (specimen) increases, so does its wear resistance.

3.3. Examination of Corrosion Resistance Properties

The electrochemical results obtained from short-term exposure of the specimens to corrosive environments are presented in Fig. 9. The diagrams in Fig. 9 are the plots of changes in the open-circuit potential versus time of immersion in the 3.5% NaCl solution. The open-circuit potential of the uncoated steel (S1) had dropped steadily during the immersion. The steel exhibits a declining open-circuit potential over the 16 hours of immersion without becoming passive. This decline is due to chloride ions' absorption, oxygen concentration changes, and dissolution of oxides formed on the surface [24]. This indicates the continuous dissolution of the steel in this corrosive solution.

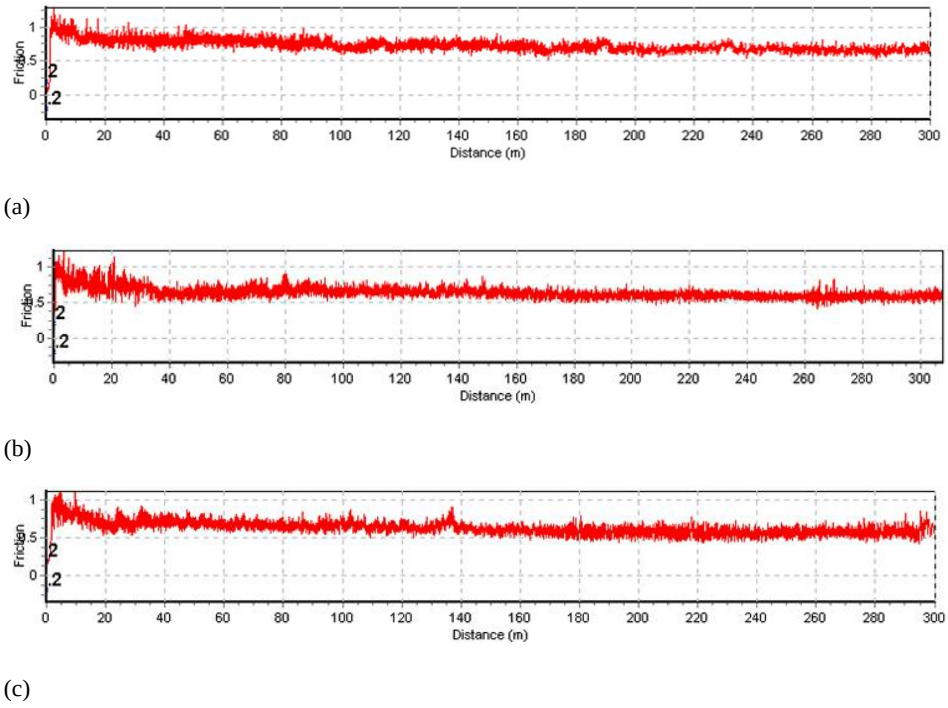

Fig. 8. Plots of friction coefficient versus sliding distance for the specimens (a) S2, (b) S3, and (c) S4

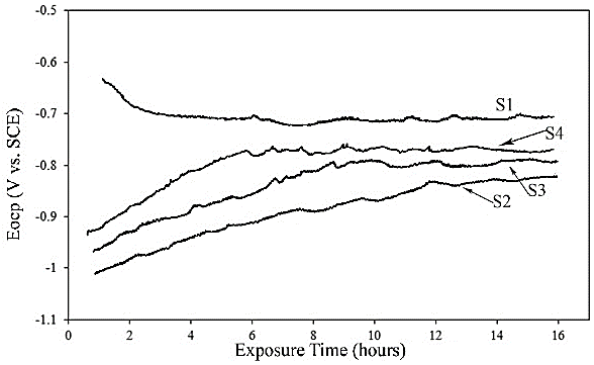

Fig. 9. The open-circuit potential of the specimens in terms of immersion time in 3.5% NaCl solution at 25°C

This dissolution occurs because of corrosive chloride ions and oxygen in the solution. The performance of the specimens S2, S3, and S4 is entirely different from that of uncoated steel (S1). The open-circuit potential of the steel with composite coating increases during the immersion until reaching a constant level. This could be due to the reduced active surface of the composite coating because of SiC particles that replace the Al particles.

The cyclic polarization curves of the specimens S2, S3, and S4 are drawn in Fig. 10. As can be seen, all three curves have similar trends. The information extracted from these curves is presented in Table 3. There are some differences in the E_{corr} values of S2, S3, and S4, related to the amount of SiC particles in the composite coating.

The corrosion resistance properties of coatings were investigated using the polarization method. Figure 10 shows the potentiodynamic curves of uncoated steel and coatings S2, S3, and S4. It should be noted that the immersion time was set to 15 hours to ensure that the observed corrosion properties are related to the interface of the coating with the base metal. As shown in Fig. 10, the Al/SiC composite coatings showed higher corrosion resistance than the uncoated steel. Steel has a higher corrosion potential (E_{ocp}) than composite coatings. The electrochemical information extracted from the potentiodynamic diagrams by curve fitting at their Tafel region is presented in Table 3. Using the I_{corr} values, the corrosion rate can be obtained using the following equation and Faraday's law:

$$C.R = \frac{3.27\, I_{corr}\, E.W}{\rho} \quad (1)$$

Table 3. Electrochemical information extracted from the potentiodynamic diagrams

Samples	E_{corr} (V vs SCE)	I_{corr} (μA/cm²)	C.R (μm/year)
S1	-710	25	195
S2	-860	11	128
S3	-803	8	110
S4	-780	5	95

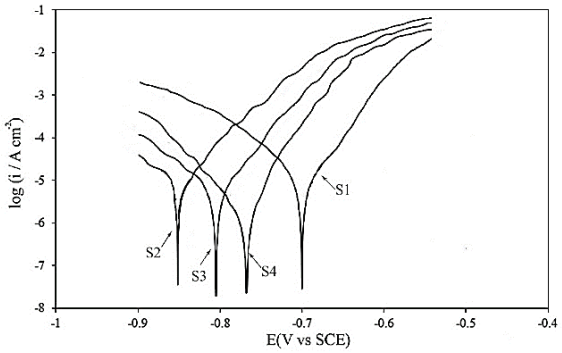

Fig. 10. Potentiodynamic diagram of the specimens for exposure to 3.5% NaCl solution at 25°C

In Eq. (1), C.R is the corrosion rate in terms of (μm/year), and I_{corr} is the corrosion current density in terms of (μA/cm^2). Also, E.W is the equivalent weight (g/mol), and ρ is density (g/cm^3).

The results presented in Table 3 clearly show that the uncoated steel has a higher corrosion rate than the Al/SiC composite coating. These results indicate that while the uncoated steel is sensitive to corrosive environments, the coated steel gains a significant level of corrosion protection from its coating. In uncoated steel, the corrosion current increases with the potential, indicating that corrosion occurs without a passive layer. However, the composite-coated steel exhibits a level of passive protection under anodic polarization. The presence of more SiC particles in the coating leads to reduced corrosion current and a slower corrosion rate, probably due to the blockage of corrosive solutions from entering the substrate-coating interface. Thus, it can be stated that the Al/SiC composite coatings increase the corrosion resistance of steel in the corrosive environment of 3.5% NaCl. A higher amount of SiC particles in the composite coating results in a lower corrosion rate.

EIS may be used to explore the corrosion behavior of an Al/SiC composite coating on a steel substrate over various exposure durations. Figure 11 shows the Nyquist plots and the corresponding equivalent circuit of the specimen S4 for six hours, 24 hours, three days, seven days, and 24 days of exposure to the corrosive solution. The Nyquist plot for 6 hours of exposure has two semicircles. Therefore, it can be stated that the system has two time constants. The time constant at high frequencies is related to the coating, and the one at low frequencies is related to the corrosion in the coating [2, 25]. In the equivalent circuit, the electrical resistance between the working and reference electrodes is Rs, the resistance of the pores of the coating is R_p, the constant phase element (CPE) capacitance is C_c, the charge transfer resistance is R_{ct}, and the double layer capacitance is C_{dl}. The parameters R_p and C_c are related to coating defects at high-frequency cycles and the parameters R_{ct} and C_{dl} are related to corrosion in the coating at low-frequency cycles [24].

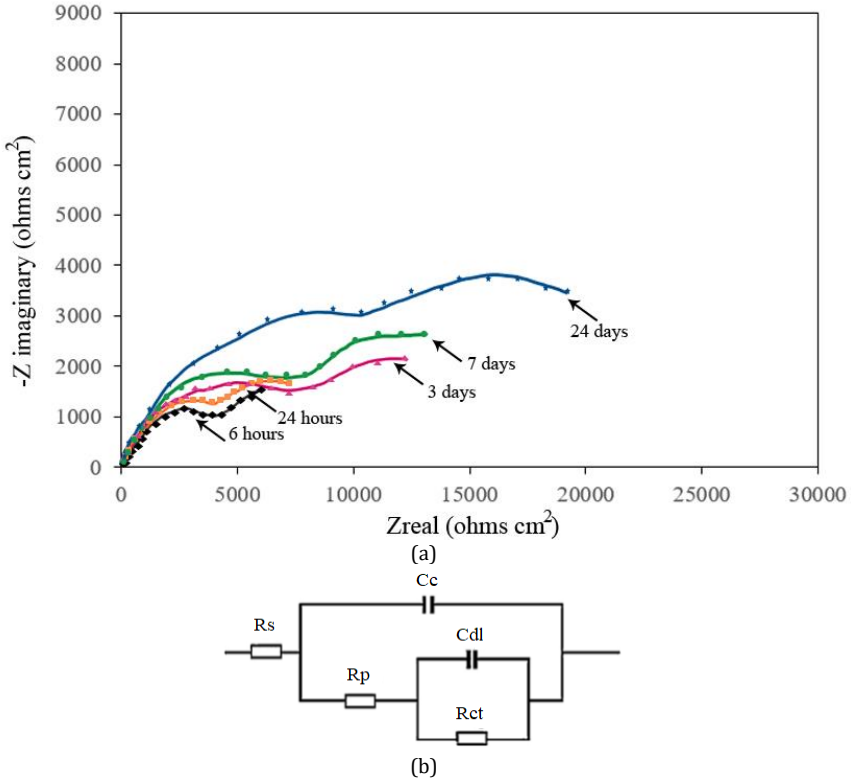

Fig. 11. (a) Nyquist spectra of the specimen S4 for 6 hours, 24 hours, three days, seven days, and 24 days of exposure (b) equivalent circuit

Table 4. Impedance parameters for S4 sample steels in 3% NaCl solution

Exposure time	R_s (Ω.cm²)	R_p (kΩ.cm²)	R_{ct} (kΩ.cm²)	Cc (µF.cm^{-2})	C_{dl} (µF.cm^{-2})
6 h	6	4.1	8.5	40	254
24 h	4	5.3	11.1	74	161
3 days	7	7.8	15.4	91	115
7 days	6	8.2	17.5	122	92
24 days	5	10.6	23.1	145	71

The electrolyte can penetrate the coating through the pores, causing corrosion in its active areas. This occurs in a capacitance observed at low frequencies. The electrolyte is less likely to corrode the substrate since the Al/SiC composite is more active than the steel substrate upon reaching it.

The parameters extracted from the simulation of impedance diagrams with equivalent circuits are presented in Table 4.

As in Table 4, the C_{dl} values decrease with increasing exposure time. Therefore, it can be stated that the area inside the coating that is exposed to the corrosive solution decreases with the immersion time. This is because the pores get blocked by the corrosion products as time passes. Also, the C_c value increases with increasing immersion time. This indicates an increase in the area in the coating exposed to corrosive electrolytes because of the increased area of the pore walls. As the immersion time increases, the accumulation of corrosion products in the pores and their blockage increases R_p.

4. Conclusions

The results obtained in this study can be summarized as follows:

1- The composite-coated specimen created with one hole in the rod (S3) had 22.1% better wear resistance than the specimen with the aluminum coating (S2). Correspondingly, the composite-coated specimens created with two holes in the rod (S4) had 16.2% better wear properties than S3.

2- Lower amounts of SiC particles in the process led to the increased presence of smaller particles in the coating.

3- The specimen S3 showed a more uniform distribution of SiC particles in its composite coating than S4. This observation indicates that the process conditions for various configurations of the holes in the aluminum rod (i.e., different SiC volume percentages) should be optimized separately.

4- The deposition of aluminum coating on the steel substrate increased its corrosion resistance. Furthermore, Al/SiC composite coating showed better corrosion resistance (lower corrosion rate) than the pure aluminum coating.

5- The examination of electrochemical impedance showed that two time constants emerge in the Nyquist plots.

5. Declarations

5.1. Ethical Approval

Not applicable because this article does not contain any studies with human or animal subjects.

5.2. Consent to Participate

Not applicable.

5.3. Consent to Publish

Not applicable.

5.4. Funding

No funding was received for conducting this study.

5.5. Competing Interests

The authors have no conflicts of interest to declare relevant to this article's content.

5.6. Availability of Data and Materials

The datasets used and analyzed during the current study are available from the corresponding author on reasonable request.

References

[1] Aboudi, J., Pindera, M.-J. & Arnold, S.M., 1999. Higher-order theory for functionally graded materials. *Composites Part B: Engineering, 30* (8)**,** pp.777-832.

[2] Ma, Z., Pilchak, A., Juhas, M. & Williams, J., 2008. Microstructural refinement and property enhancement of cast light alloys via friction stir processing. *Scripta Materialia, 58* (5)**,** pp.361-366.

[3] Puli, R. & Ram, G.J., 2012. Microstructures and properties of friction surfaced coatings in AISI 440c martensitic stainless steel. *Surface and Coatings Technology, 207***,** pp.310-318.

[4] Liu, S., Bor, T., Van Der Stelt, A., Geijselaers, H., Kwakernaak, C., Kooijman, A., Mol, J., Akkerman, R. & Van Den Boogaard, A., 2016. Friction surface cladding: An exploratory study of a new solid state cladding process. *Journal of materials processing technology, 229***,** pp.769-784.

[5] Nie, J., Morton, A. & Muddle, B., Aluminium alloys-their physical and mechanical

properties volume 28-2004. Materials Forum, 2004.
[6] Shafiei-Zarghani, A., Kashani-Bozorg, S. & Zarei-Hanzaki, A., 2011. Wear assessment of al/al2o3 nano-composite surface layer produced using friction stir processing. *Wear, 270* (5-6)**,** pp.403-412.
[7] Tahmasbi, K., Mahmoodi, M. & Tavakoli, H., 2019. Corrosion resistance of aluminum alloy aa7022 wire fabricated by friction stir extrusion. *Transactions of Nonferrous Metals Society of China, 29* (8)**,** pp.1601-1609.
[8] Bedford, G., 1990. Friction surfacing for wear applications. *Metals and Material***,** pp.702-705.
[9] Puli, R. & Ram, G.J., 2012. Dynamic recrystallization in friction surfaced austenitic stainless steel coatings. *Materials characterization, 74***,** pp.49-54.
[10] Rao, K.P., Sankar, A., Rafi, H.K., Ram, G. & Reddy, G.M., 2013. Friction surfacing on nonferrous substrates: A feasibility study. *The International Journal of Advanced Manufacturing Technology, 65* (5)**,** pp.755-762.
[11] Sahin, Y. & Acılar, M., 2003. Production and properties of sicp-reinforced aluminium alloy composites. *Composites Part A: Applied Science and Manufacturing, 34* (8)**,** pp.709-718.
[12] Miracle, D., 2005. Metal matrix composites–from science to technological significance. *Composites science and technology, 65* (15-16)**,** pp.2526-2540.
[13] Akovali, G., 2001. *Handbook of composite fabrication*. iSmithers Rapra Publishing.
[14] Paciej, R. & Agarwala, V., 1986. Metallurgical variables influencing the corrosion susceptibility of a powder metallurgy sicw/al composite. *Corrosion, 42* (12)**,** pp.718-729.
[15] De Salazar, J., Urena, A., Manzanedo, S. & Barrena, M., 1998. Corrosion behaviour of aa6061 and aa7005 reinforced with al2o3 particles in aerated 3.5% chloride solutions: Potentiodynamic measurements and microstructure evaluation. *Corrosion Science, 41* (3)**,** pp.529-545.
[16] Ranjan, R. & Das, A.K., 2022. Enhancement of mechanical and corrosion protection properties of different substrates after friction surfacing: A concise review. *Materials Today: Proceedings, 57***,** pp.2111-2115.
[17] Bararpour, S.M., Jamshidi Aval, H. & Jamaati, R., 2020. Effect of non-isothermal aging on microstructure and mechanical properties of friction surfaced aa5083-15wt%zn composites. *Surface and Coatings Technology, 384***,** pp.125307.
[18] Sahoo, D.K., Guna, P. & Deepan, S., 2022. Performance analysis on deposition of aluminium 6063 over en8 medium carbon steel by friction surfacing. *Materials Today: Proceedings*.
[19] Sahoo, D.K., Nivas Chari, A. & Sivakrishna Reddy, A., 2020. Optimization & characterization of friction surfaced coatings of aa6063 aluminium alloy over aisi316 stainless steel substrate. *Materials Today: Proceedings, 23***,** pp.565-572.
[20] Gnanasekaran, M., Mohan, K., Kumaravel, A. & Magibalan, S., 2020. Characterization, corrosion behavior, effect of temperature and inhibition studies on aa6351 frictional surfaced mild steel. *Journal of Materials Research and Technology, 9* (6)**,** pp.16080-16092.
[21] Yu, M., Zhao, H., Zhang, Z., Zhou, L., Song, X. & Ma, N., 2021. Texture evolution and corrosion behavior of the aa6061 coating deposited by friction surfacing. *Journal of Materials Processing Technology, 291***,** pp.117005.
[22] Verma, A.S. & Suri, N.M., 2015. Corrosion behavior of aluminum base particulate metal matrix composites: A review. *Materials Today: Proceedings, 2* (4-5)**,** pp.2840-2851.
[23] Mishra, R.S., Ma, Z. & Charit, I., 2003. Friction stir processing: A novel technique for fabrication of surface composite. *Materials Science and Engineering: A, 341* (1-2)**,** pp.307-310.
[24] Tavakoli, H. & Khoie, S.M., 2010. An electrochemical study of the corrosion resistance of boride coating obtained by thermo-reactive diffusion. *Materials Chemistry and Physics, 124* (2-3)**,** pp.1134-1138.
[25] Liu, C., Bi, Q. & Matthews, A., 2001. Eis comparison on corrosion performance of pvd tin and crn coated mild steel in 0.5 n NaCl aqueous solution. *Corrosion Science, 43* (10)**,** pp.1953-1961.